2024 IEEE International Conference on Robotics and Automation (ICRA 2024)
May 13-17, 2024. Yokohama, Japan

Development of a 3-RRS Micromanipulator Based on Origami-Inspired Spherical Joint

Haoqi Han, Xiaoming Liu, *Member, IEEE,* Yan Chen, Hao Pang, Xiaoqing Tang, Dan Liu, Qiang Huang, *Life Fellow, IEEE* and Tatsuo Arai, *Life Fellow, IEEE*

Abstract— **In recent years, micromanipulation technology has achieved extensive applications in industry and life science. Improving the precision and bandwidth of the micromanipulator and simultaneously reducing size, weight, and cost pose significant challenges to the existing micromanipulator design and fabrication methods. Here, we propose a 3-RRS micromanipulator with an origami-inspired spherical joint based on the PC-MEMS process, aiming for miniaturization and cost-effectiveness. The spherical joint allows rotations of 140° around the x-axis approximately, 140° around the y-axis approximately, and 20° around the z-axis approximately. The micromanipulator has weights of 0.8 g, dimensions of 16 mm × 16 mm × 22 mm, and workspace of 0.7 mm^3. The end platform of the micromanipulator can be equipped with various effectors to accomplish different kinds of tasks. Experimental results validated its high precision and bandwidth, exhibiting its potential to perform intricate micromanipulation tasks.**

I. INTRODUCTION

In recent years, there has been an increasing demand for micromanipulation in the industry and life science, particularly in procedures like minimally invasive surgery and cell operations. Micromanipulators play a crucial role in facilitating the safe and efficient execution of these tasks. These manipulators are designed for various applications, including cell manipulation [1], surgical defibrillation [2], and even substituting manual surgery procedures [3]. The key challenge in designing micromanipulators revolves around the selection of suitable actuators [4] and parallel mechanisms [5]. Designers aim for actuators that possess several advantages such as lightweight construction, high bandwidth, large energy density, and extensive displacement range. Piezoelectric actuators have gained significant popularity among designers due to their ability to provide extremely small motions with micrometer-level position resolution [6]. By incorporating parallel mechanisms, micro motions with multiple degrees of freedom can be achieved.

Han and Riviere et al. successfully developed a micro Gough-Stewart platform employing six individual piezoelectric linear actuators with integral feedback sensors. This platform exhibited a cylindrical workspace measuring at least 6 mm in length and 4 mm in diameter [2]. In 2013, Becker and Riviere et al. introduced a 3-DOF piezoelectric manipulator with a 400 um range of motion, 1 N force capability, and a bandwidth over 100 Hz. It can reduce the positional error of a surgeon's handheld movements by varying degrees, ranging from 32% to 52%, during surgical procedures [7-9]. Kallio devised a piezohydraulic parallel micromanipulator with a workspace measuring 1.5 mm × 0.6 mm × 0.25 mm [10]. These designs primarily focus on single end-effector manipulators. However, to achieve superior manipulation capabilities, the concept of a two-finger manipulator was proposed. Nakazato designed a micromanipulator driven by memory alloy in 2005, capable of grasping particles with a diameter of 35 microns and exerting a grasping force of 180 mN [11]. In 2007, Koseki developed a two-finger micromanipulator driven by piezoelectric actuators, featuring a main structure made of propylene plastic and a glass needle at the actuator's end [12].

In 2009, Ramadan et al. developed a chopstick-like hybrid-structure two-fingered micromanipulator hand [13]. This hand employed two spatial 3-PRS parallel mechanisms in series connection, enabling high-precision and dynamic particle grasping tasks. Through extensive experiments, they demonstrated pick-and-place actions of microspheres ranging from 40 to 60 um within a time frame of 1s [14][15]. In recent years, further advancements have been made in micromanipulator design. Among these, the 3-RRS robot, as a representative parallel robot, stands out due to its numerous advantages, including robust load capacity, high efficiency, precise end effector control, minimal motion inertia, high speed, and stable motion[13-15]. We anticipate that this structure can assume a more prominent role in the field of micromanipulation, which demands exceptional precision.

However, as the sizes of micromanipulators continue to shrink, challenges related to part accuracy and process costs become increasingly perplexing. Furthermore, parallel robots constructed using flexible links face inherent stiffness and damping issues at the joints. Designing small mechanisms with low-damping flexible joints has emerged as a significant

This work was supported by the National Natural Science Foundation of China under Grant 62273052, the Beijing Natural Science Foundation under Grant IS23062, China Postdoctoral Science Foundation under Grant 2022M710378 and the Grant-in-Aid for Scientific Research under Grant 22H01441 from the Ministry of Education, Culture, Sports, Science and Technology of Japan. *(Corresponding author: Xiaoming Liu.*)

H. Han, Y. Chen, H. Pang, X. Tang, D. Liu, X. Liu, Q. Huang, and T. Arai are with the Key Laboratory of Biomimetic Robots and Systems, Ministry of Education, State Key Laboratory of Intelligent Control and Decision of Complex System, Beijing Advanced Innovation Center for Intelligent Robots and Systems, and School of Mechatronical Engineering, Beijing Institute of Technology, Beijing 100081, China (e-mail: liuxiaoming555@ bit.edu.cn)

H. Han is also with the Department of Micro-Nano Electronics, Shanghai Jiao Tong University, Shanghai 200240, China (e-mail: hhq-2018@foxmail.com).

T. Arai is also with Center for Neuroscience and Biomedical Engineering, The University of Electro-Communications, Tokyo 1828585, Japan.

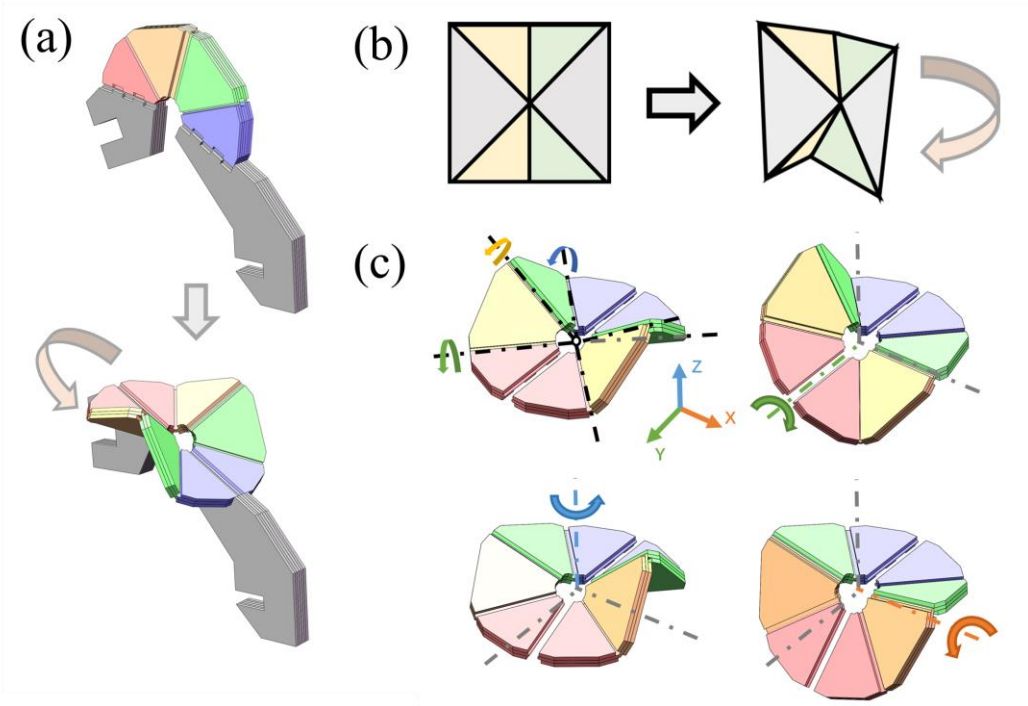

Fig 1. Schematic of the origami-inspired spherical joint. (a) The manufacturing process of the spherical joint. The spherical joint consists of two layers of standard linkage sub-laminates. Once released, it will be assembled and securely bonded using adhesive. (b) A spherical joint folded by paper. (c) Motion of origami-inspired spherical joint. The spherical joint exhibits excellent motion in three rotational directions.

challenge. Researchers at the Wyss Institute have developed a bulk-machined Pop-up MEMS process for creating microscale machines [16-17]. McClintock successfully developed a millimeter-scale parallel manipulator known as MilliDelta in 2018 [5], measuring a mere 15 mm × 15 mm × 20 mm. MilliDelta exhibits high-speed movement across three degrees of freedom and possesses a workspace of 7.01 mm^3. In 2020, Suzuki developed a surgical robot called mini-RCM with a mass of 2.4 g and a size of 50 mm × 70 mm × 50 mm [18]. The mini-RCM features a positional precision of 26.4 μm and a load capacity of 27 mN. It exhibits potential for application in teleoperated microsurgery.

In this paper, we propose a 3-RRS micromanipulator based on a new origami-inspired spherical joint based on the PC-MEMS process. Different from MilliDelta, we integrate rotational degrees of freedom at the end effector and employ probe motion amplification. These designs improve the applicability of the manipulator in the field of micromanipulation. The design and assembly of the micromanipulator are comprehensively described in Section II. In Section III, an analysis of the inverse kinematics of the micromanipulator is presented. The experiments and discussions regarding the performance of the micromanipulator are presented in Section IV. Conclusions are in Section V.

II. DESIGN

A. Origami-Inspired Spherical Joint

In related studies, researchers have utilized polymer wires or precisely machined microsphere joints as spherical joints [2][15]. However, manufacturing and assembling these joints is difficult. In addition, polymer wires may induce motion deviations during movement. Typically, the origami-inspired spherical joint can be folded as Fig. 1a. It can provide three degrees of freedom for rotational motion. However, it cannot perform rotations perpendicular to the paper plane in its initial position.

To realize the spherical joint, we construct the spherical joint using three rotating joints. Specifically, the second rotating axis was offset by approximately 36° to enable a rotational range of about 20° around the z-axis. As a result, the constructed spherical joint demonstrates exceptional mobility in all three rotational directions, as depicted in Fig. 1c. The spherical joint is composed of two standard linkage sub-laminates [19], containing six linkages connected by six revolute joints. Once released, it will be deployed by a 90° fold and assembled into the overall structure.

Through testing, it is determined that this origami-inspired spherical joint can rotate approximately 140° around the x-axis, approximately 140° around the y-axis, and approximately 20° around the z-axis. In contrast to conventional micro-spherical joints, our spherical joint is more amenable to mass manufacturing while ensuring considerable motion precision.

B. The 3-RRS Micromanipulator

This work presents a parallel micromanipulator based on the origami-inspired spherical joint. Typically, designing a manipulation device requires a minimum of three degrees of freedom. In the field of micromanipulation, the rotational degree of freedom allows for the adjustment of the probe's angle of contact with microparticles. This capability enhances

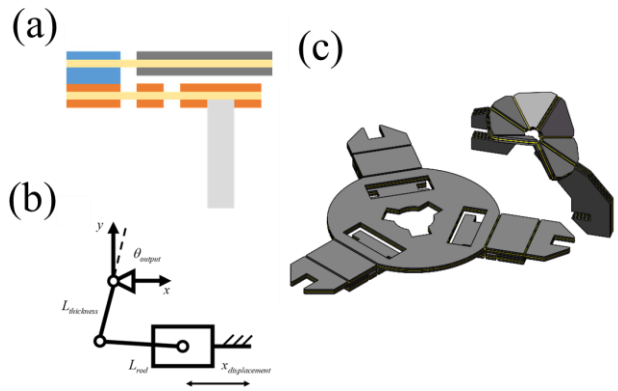

Fig 2. Schematic of parallel platform. (a) Practical model. The base of the manipulator consists of two layers of standard linkage sub-laminates, with parameter $L_{thickness}$ set to 0.3 mm. (b) Theoretical model. The motion amplifier comprises a slider-linkage structure that converts the motion of the piezoelectric actuator into joint rotations. (c) The parallel platform consists of motion amplification platform and motion transmission chain.

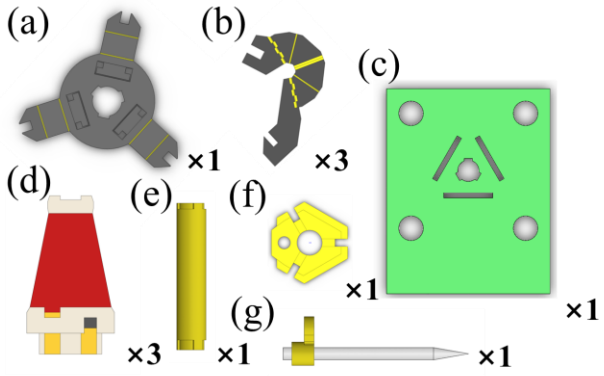

Fig 3. The components of the micromanipulator. (a) The base with three amplifications. (b) Spherical joint linkage. (c) Support PCB board. (d) Piezoelectric actuator. (e) 3D-printed pillar. (f) The end platform. (g) The end-effector probe.

the gripping of microparticles and improves overall work efficiency. This grants the 3-RRS parallel mechanism a significant advantage in micromanipulation.

The overall design is based on CAD software (SolidWorks and AutoCAD). The traditional 3-RRS parallel mechanism is composed of three identical motion branches, each consisting of a spherical joint and two revolute joints. To achieve miniaturization, we utilized the PC-MEMS fabrication [16], resulting in a compact structure measuring approximately 16 mm × 16 mm × 22 mm. The manipulator comprises a base, three piezoelectric actuators, a 3-RRS parallel mechanism, and a probe. The 3-RRS parallel mechanism incorporates a base equipped with an amplification mechanism, three linkages featuring spherical hinges, and an end platform produced using high-precision 3D printing.

The base of the manipulator is composed of three slider-crank mechanisms, as shown in Fig. 2a. These mechanisms serve to convert the displacement of the piezoelectric actuators into rotational motion [5]. The rotational motion, combined with the parallel mechanism, provides the end platform with two rotational degrees and one translational degree of freedom. The amplification of motion through the probe provides a workspace of approximately 0.7 mm^3. By manipulating the rotational degree of freedom, the manipulator can achieve optimal positioning and manipulation of the microparticles, leading to enhanced precision and productivity in micromanipulation tasks.

C. Final Assembly

The overall weight of the manipulator is approximately 0.8 g. The manipulator is composed of a total of 11 components, including a base with three amplifications, three spherical joint linkages, a support PCB board, three piezoelectric actuators, a 3D-printed pillar, an end platform, and an end-effector probe, as shown in Fig. 3. The effective working length of the piezoelectric actuator is designed to be 10 mm. It can provide a motion range of approximately 400 um under 200 V. The fabrication of piezoelectric actuators is referred to [4][20]. The pillar and end platform are manufactured using high-precision 3D printing to ensure the overall accuracy of the mechanism. The parallel mechanism is manufactured by the PC-MEMS fabrication process [16]. The rigid layer is a composite of three layers of carbon fiber prepreg (USN03000) at orthogonal angles. After laser cutting, layers of material are assembled in sequence. Then the composite will be cured using sheet adhesive (LF0100, Dupont) under conditions of 1kg/cm^2 and a temperature of 200 °C. Finally, a second laser-cutting process is employed to obtain four individual components.

After preparing all the materials, the micromanipulator will be assembled by CA adhesive (CA40H, Scotch-Weld, 3M). Firstly, the piezoelectric actuators and the pillar are secured onto the circuit board by specially designed positioning tools. Subsequently, the base platform, which includes the motion amplification mechanism, is carefully attached to the pillar to ensure proper alignment and stability. After unfolding, the spherical joints are initially attached to the end platform and subsequently attached to the base platform by CA adhesive. A customized probe will be installed at the end to be used for micromanipulation tasks. At the bottom of the piezoelectric actuators, connecting pads are designed to connect the electrodes to the circuit board using conductive adhesive. The control signals will be put on the parallel mechanism through the circuit board.

III. WORKSPACE ANALYSIS

A. Inverse Kinematic

To drive the manipulator and perform operational tasks, analysis of the inverse kinematic is necessary. From Fig. 4a, the posture of the mobile plate is typically described using the ZXZ rotation transformation [13][21].

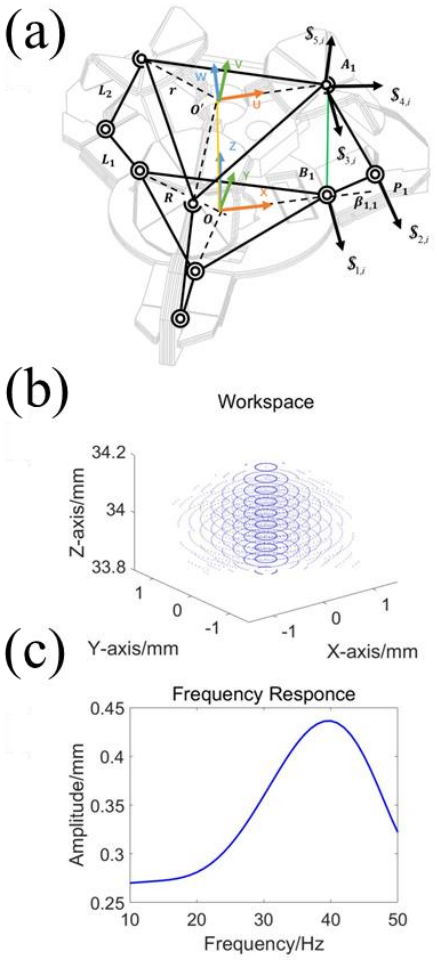

Fig 4. (a) The geometrical structure of the 3-RRS parallel mechanism. (b) Workspace of the 3-RRS micromanipulator. (c) Frequency Response of the 3-RRS micromanipulator.

$$R_m = \begin{bmatrix} u_x & v_x & w_x \\ u_y & v_y & w_y \\ u_z & v_z & w_z \end{bmatrix} = \begin{bmatrix} c\psi c\phi - s\psi c\theta s\phi & -c\psi s\phi - s\psi c\theta c\phi & s\psi s\theta \\ s\psi c\phi + c\psi c\theta s\phi & -s\psi s\phi + c\psi c\theta c\phi & -c\psi s\theta \\ s\theta s\phi & s\theta c\phi & c\theta \end{bmatrix} \quad (1)$$

For a single kinematics chain in this mechanism, we can describe it as:

$$\overline{OO'} + \overline{O'A_i} = \overline{OB_i} + \overline{B_iP_i} + \overline{P_iA_i}, i = 1,2,3 \quad (2)$$

Considering that the rotating joints are parallel and perpendicular to the linkage, we can obtain the constraints equation of the mobile plate by taking the dot product with $\vec{c_i} = [sin\phi_i \quad -cos\phi_i \quad 0]^T$ parallel to the rotational joint.

$$\left(\overline{OO'} + \overline{O'A_i}\right)^T \cdot \vec{c_i} = 0 \quad (3)$$

Here we can prove that

$$\begin{bmatrix} sin\phi_i \\ -cos\,\phi_i \\ 0 \end{bmatrix}^T \begin{bmatrix} r\,cos\,\phi_i\,u_x + r\,sin\,\phi_i\,v_x + X_{O'} \\ r\,cos\,\phi_i\,u_y + r\,sin\,\phi_i\,v_y + Y_{O'} \\ r\,cos\,\phi_i\,u_z + r\,sin\,\phi_i\,v_z + Z_{O'} \end{bmatrix} = 0 \quad (4)$$

The relationship between the coordinates and angles of the mobile plate can be described as

$$\begin{cases} X_{O'} = \frac{r}{2} sin\,2\psi(cos\,\theta - 1) \\ Y_{O'} = \frac{r}{2} cos\,2\psi(cos\,\theta - 1) \\ \psi = -\phi \end{cases} \quad (5)$$

The coordinates of the end effector are

$$\boldsymbol{E} = \begin{bmatrix} u_x & v_x & w_x \\ u_y & v_y & w_y \\ u_z & v_z & w_z \end{bmatrix} \begin{bmatrix} 0 \\ 0 \\ L_{end} \end{bmatrix} + \begin{bmatrix} X_{O'} \\ Y_{O'} \\ Z_{O'} \end{bmatrix} = \begin{bmatrix} X \\ Y \\ Z \end{bmatrix} \quad (6)$$

To effectively control the micromanipulator and accomplish specific and intricate tasks, it is crucial to precisely determine the input signals applied to the piezoelectric actuators based on a given location of the mobile plate.

According to (2), we can obtain the coordinates of points A_i. The length of $\overline{B_iA_i}$ can be expressed as

$$L_{3,i} = \sqrt{(x_{A_i} - x_{B_i})^2 + (y_{A_i} - y_{B_i})^2 + (z_{A_i} - z_{B_i})^2} \quad (7)$$

The direction angle $\beta_{2,i}$ for $\overline{B_iA_i}$can be described as

$$\beta_{2,i} = arccos\left(\frac{\overline{B_iA_i} \cdot \overline{B_iO_i}}{|\overline{B_iA_i}||\overline{B_iO_i}|}\right) \quad (8)$$

The input angles for the rotational joints of the base are given by:

$$\beta_{1,i} = \beta_{2,i} - arccos\left(\frac{{L_{1,i}}^2 + {L_{3,i}}^2 - {L_{2,i}}^2}{2L_{1,i}L_{3,i}}\right) \quad (9)$$

These rotational angles are ultimately converted into the displacement of the piezoelectric actuators.

B. Workspace Analysis Result

In Fig. 4b, the results of the workspace are shown in the form of the coordinates of the end of the probe. The length of the probe is 30 mm. Based on the inverse kinematics and experimental data, the manipulator can achieve a feed motion of approximately 0.5 mm along the Z-axis and has a motion area of approximately 2.3 mm in the XY plane. The total workspace is approximately 0.7 mm^3, which is typically determined by the length of the probe.

In practical applications, the motion of the probe is achieved by controlling the two rotational parameters and position along the Z-axis of the mobile plate. The rotational parameters represent the deviation angle between the probe and the Z-axis and the rotation angle around the Z-axis. By adjusting these control inputs, the probe can be driven to move

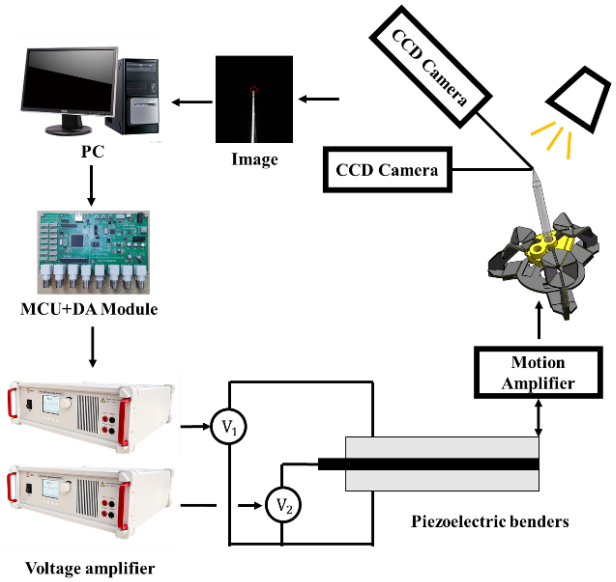

Fig 5. The experimental setup of 3-RRS micromanipulator.

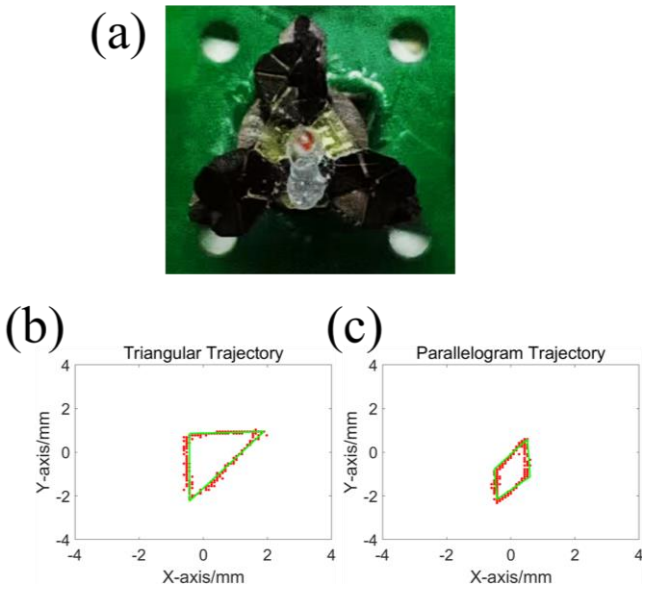

Fig 6. (a) The top view of the micromanipulator. (b) The micromanipulator follows the desired triangular trajectory. (c) The micromanipulator follows the desired parallelogram trajectory. The green line represents the desired trajectory, and the red dot represents the actual motion path.

at the desired angle and depth, enabling precise positioning and manipulation during real-world tasks.

IV. EXPERIMENTAL RESULTS AND DISCUSSION

A. System Setup

The experimental setup is used to determine the workspace of the 3-RRS micromanipulator, measure its frequency response, and validate its high control precision. The experimental setup is shown in Fig. 5, the 3-RRS micromanipulator is fixed to an optical vibration cancellation stage, and control commands are sent from a PC to an amplifier via a DAC module. The power amplifier (ATA-2022B ATA-309, Aigtek, China) then amplified the voltage to the driving voltage for driving the piezoelectric actuators. For capturing the motion of the end, A setup of two cameras (MV-CA020-10UM MV-CA016-10UM, Hikvision, China) in the x-y plane orthogonally is employed to capture images for analysis.

B. Workspace Test

To determine the workspace of the micromanipulator, we actuated two of the piezoelectric actuators with maximum positive and negative drive voltages, while actuated the other piezoelectric actuator with the opposite voltage, and then the workspace of the manipulator along the motion direction of the piezoelectric actuator with the opposite voltage can be determined. In addition, we actuated all piezoelectric actuators with maximum positive and negative drive voltages to determine the workspace of the micromanipulator in the z-axis direction, thus determining the workspace of the manipulator based on the inverse kinematics. The images of the motion of the end were captured by two cameras at 100 frames per second. The experimental results indicate that, with a 3cm probe and 80 V voltage drive, the workspace of the micromanipulator, as shown in Fig. 4b, presented a movement range of approximately 0.5 mm in the z-axis direction, while in the x and y-axis directions, it presented a gradually diminishing circular space with a diameter of approximately 2.3 mm.

C. Frequency Response Test

To measure the frequency response characteristics of the micromanipulator, each piezoelectric actuator was individually driven by a 50 V sine wave signal. The frequency of the sine wave gradually increased from 10 to 50 Hz, and the motion amplitude of the end effector was recorded with a camera at 240 frames per second, and then we can measure the frequency response characteristics of the manipulator, which is shown in Fig. 4c. The experimental results exhibit that when the frequency was set to 40 Hz approximately, the micromanipulator had the maximum motion amplitude, which was 0.43 mm approximately.

D. Motion Control Test

To validate the high control precision of the micromanipulator, we generated control signals based on the inverse kinematic model to drive the manipulator along the desired trajectory. These experiments were conducted under open-loop control. We successfully controlled the micromanipulator to follow both the triangular and parallelogram trajectories, which are shown in Fig. 6. For specific videos, please refer to the supplementary materials.

E. Discussion

The workspace of the micromanipulator is determined through the experiment. In addition, we measured the frequency response of the manipulator through experiment. The high control precision is also validated by controlling the manipulator to follow desired triangular and parallelogram trajectories. Based on the experimental results, the 3-RRS micromanipulator can be controlled along the desired trajectories within a workspace of approximately 0.7 mm^3.

The manipulator is capable of following periodic trajectories with frequencies as high as 40 Hz, meeting the practical requirements for complex micromanipulation tasks.

V. CONCLUSION AND FUTURE WORK

In this work, we proposed a new origami-inspired spherical joint developed by the PC-MEMS process with the capacity of rotating 140° around the x-axis, 140° around the y-axis, and 20° around the z-axis. Based on the new spherical joint and PC-MEMS process, we introduced the 3-RRS micromanipulator with a lightweight and compact design, capable of performing diverse tasks using different end effectors. Through experiments, the workspace and bandwidth have been validated. The manipulator equipped with a 3 mm probe can afford a workspace of about 0.7 mm^3 with a resonant frequency of approximately 40 Hz. Additionally, trajectory tracking experiments have confirmed the manipulator's great operability and controllability. Manufactured through the PC-MEMS process, the micromanipulator is characterized by its ease of production and cost-effectiveness. The micromanipulator shows lightweight and user-friendly features, offering vast potential applications in the field of biomedicine.

Future work includes optimizing the size, weight, workspace, and bandwidth of the manipulator. Furthermore, the control system for the manipulator will be improved. We will establish a high-precision visual servo closed-loop control system for the micromanipulator, enabling its operation at the micro-scale. Additionally, microparticle grasping experiments are planned to validate the manipulator's potential in the field of micromanipulation.

ACKNOWLEDGMENT

This work was supported by the National Natural Science Foundation of China under Grant 62273052, the Beijing Natural Science Foundation under Grant IS23062, China Postdoctoral Science Foundation under Grant 2022M710378 and the Grant-in-Aid for Scientific Research under Grant 22H01441 from the Ministry of Education, Culture, Sports, Science and Technology of Japan.

REFERENCES

[1] E. Avci, "High-speed automated manipulation of microobjects using a two-fingered microhand," *IEEE Trans. Ind. Electron.*, vol. 62, no. 2, pp. 1070-1079, 2014.

[2] Y. Han, A. Routray, J. O. Adeghate, R. A. MacLachlan, J. N. Martel, and C. N. Riviere, "Monocular vision-based retinal membrane peeling with a handheld robot," *J Med Device*, vol. 15, no. 3, p. 031014, 2021.

[3] S. DiMaio, M. Hanuschik, and U. Kreaden, "The da Vinci surgical system," Surgical robotics: systems applications and visions, pp. 199-217, 2011.

[4] N. T. Jafferis, M. J. Smith, and R. J. Wood, "Design and manufacturing rules for maximizing the performance of polycrystalline piezoelectric bending actuators," *SMART MATER STRUCT*, vol. 24, no. 6, p. 065023, 2015.

[5] H. McClintock, F. Z. Temel, N. Doshi, J.-s. Koh, and R. J. Wood, "The milliDelta: A high-bandwidth, high-precision, millimeter-scale Delta robot," *Sci. Robot.*, vol. 3, no. 14, p. eaar3018, 2018.

[6] R. J. Wood, E. Steltz, and R. Fearing, "Optimal energy density piezoelectric bending actuators," *Sens. Actuator A Phys.*, vol. 119, no. 2, pp. 476-488, 2005.

[7] R. A. MacLachlan, B. C. Becker, J. C. Tabarés, G. W. Podnar, L. A. Lobes, and C. N. Riviere, "Micron: an actively stabilized handheld tool for microsurgery," *IEEE Trans. Robot.*, vol. 28, no. 1, pp. 195-212, 2011.

[8] B. C. Becker, R. A. MacLachlan, L. A. Lobes, G. D. Hager, and C. N. Riviere, "Vision-based control of a handheld surgical micromanipulator with virtual fixtures," *IEEE Trans. Robot.*, vol. 29, no. 3, pp. 674-683, 2013.

[9] A. Routray, R. A. MacLachlan, J. N. Martel, and C. N. Riviere, "Real-time incremental estimation of retinal surface using laser aiming beam," in *2019 Int. Symp. Med. Robot.*, pp. 1-5.

[10] P. Kallio, M. Lind, Q. Zhou, and H. N. Koivo, "A 3-DOF piezohydraulic parallel micromanipulator," in *Proceedings. 1998 I Proc IEEE Int Conf Rob Autom.*, vol. 2: IEEE, pp. 1823-1828.

[11] Y. Nakazato, A. Sekine, H. Miyazawa, S. Takeuchi, Y. Ariga, and M. Murakawa, "Development of a micromanipulator made of diamond having reversal mechanism," *Microsyst. Technol.*, vol. 11, pp. 997-1004, 2005.

[12] Y. Koseki, T. Tanikawa, and K. Chinzei, "MRI-compatible micromanipulator; design and implementation and MRI-compatibility tests," in *2007 29th Annu Int Conf IEEE Eng Med Biol Proc.*, pp. 465-468.

[13] A. A. Ramadan, K. Inoue, T. Arai, and T. Takubo, "Design optimization of a compact 3-DOF parallel micro/nano finger manipulator," in *2006 IEEE Int Conf Intell Rob Syst.*, pp. 778-783.

[14] E. Avci, "Piezo-actuated parallel mechanism for biological cell release at high speed," *Biomed Microdevices*, vol. 17, pp. 1-10, 2015.

[15] A. A. Ramadan, T. Takubo, Y. Mae, K. Oohara, and T. Arai, "Developmental process of a chopstick-like hybrid-structure two-fingered micromanipulator hand for 3-D manipulation of microscopic objects," *IEEE Trans. Ind. Electron.*, vol. 56, no. 4, pp. 1121-1135, 2009.

[16] J. P. Whitney, P. S. Sreetharan, K. Y. Ma, and R. J. Wood, "Pop-up book MEMS," *J Micromech Microeng*, vol. 21, no. 11, p. 115021, 2011.

[17] J. B. Gafford, S. B. Kesner, R. J. Wood, and C. J. Walsh, "Microsurgical devices by pop-up book mems," in *2013 Proc. ASME Des. Eng. Tech. Conf.*, vol. 55935: American Society of Mechanical Engineers, p. V06AT07A011.

[18] H. Suzuki and R. J. Wood, "Origami-inspired miniature manipulator for teleoperated microsurgery," *Nat. Mach. Intell.*, vol. 2, no. 8, pp. 437-446, 2020.

[19] A. T. Baisch, O. Ozcan, B. Goldberg, D. Ithier, and R. J. Wood, "High speed locomotion for a quadrupedal microrobot," *Int J Rob Res*, vol. 33, no. 8, pp. 1063-1082, 2014.

[20] N. T. Jafferis, M. Lok, N. Winey, G.-Y. Wei, and R. J. Wood, "Multilayer laminated piezoelectric bending actuators: design and manufacturing for optimum power density and efficiency," *SMART MATER STRUCT*, vol. 25, no. 5, p. 055033, 2016.

[21] T. Ejima, "Development of microhand utilizing singularity of parallel mechanism," in *2013 IEEE Int Conf Intell Rob Syst*, pp. 1525-1530.